References

[1] Summerfield, M., "A Theory of Unstable Combustion in Liquid Propellant Rocket Systems," *ARS Journal*, Vol. 21, No. 5, Sept. 1951, pp. 108–114.

[2] Crocco, L., "Aspects of Combustion Stability in Liquid Propellant Rocket Motors," Part 1, *ARS Journal*, Vol. 21, No. 6, Nov. 1951, pp. 163–178.

[3] McKenna, K. J., Walker, J. H., and Winje, R. A., "Engine-Airframe Coupling in Liquid Rocket Systems," *Journal of Spacecraft and Rockets*, Vol. 2, No. 2, March-April 1965, pp. 254–256.

[4] Rubin, S., "Longitudinal Instability of Liquid Rockets Due to Propulsion Feedback (*POGO*)." *Journal of Spacecraft and Rockets*, Vol. 3, No. 8, Aug. 1966, pp. 1188–1195.

[5] Savant, C. J., Jr., "*Basic Feedback Control System Design*," McGraw-Hill, New York, 1958, pp. 124–168.

[6] MacLean, D. I. and Wagner, H. Gg, "The Structure of the Reaction Zones of Ammonia-Oxygen and Hydrazine-Decomposition Flames," *Eleventh Symposium (International) on Combustion*, The Combustion Institute, 1967, p. 871.

[7] Kestin, A. S., "Turbulent Diffusion of Heat and Mass in Catalytic Reactors for Hydrazine Decomposition," *Journal of Spacecraft and Rockets*, Vol. 7, No. 1, Jan. 1970, pp. 31–36.

[8] "Dynamic Analyses of Thrust Chambers," Interim Rept. 4600-147-1, Sept. 1968, Walter Kidde & Co., Belleville, New Jersey.

[9] Crocco, L., Grey, J., and Matthews, G. B., "Measurements of the Combustion Time Lag in a Liquid Bipropellant Rocket Motor," *Jet Propulsion*, Vol. 26, No. 1, Jan. 1956, pp. 20–25.

[10] Barrére, M., et al., "*Rocket Propulsion*," Van Nostrand, Princeton, 1960, pp. 630–632.

MARCH 1972 J. SPACECRAFT VOL. 9, NO. 3

Barrier Film Cooling Study

KURT BERMAN* AND S. J. ANDRYSIAK†
Bell Aerospace Company, Buffalo, N.Y.

Tests were conducted to evaluate the effectiveness of a liquid film barrier injected into a rocket thrust chamber with a vortex motion, insofar as heat transfer and performance were concerned. The propellant combination used was N_2O_4 and MMH. The engine, designed for a normal 450 lb thrust level at 125 psia chamber pressure, utilized a building block injector in which the core and barrier were fed separately, thus permitting independent control of the respective flow rates. The injector core pattern contained doublet and triplet elements. The chambers and nozzles were uncooled and instrumented with chromel-alumel thermocouples to obtain circumferential as well as axial heat rejection patterns. Both N_2O_4 and MMH were investigated as barrier coolants. Data were obtained showing the effect of barrier flow rate variations on performance and wall temperature at constant core flow rates and mixture ratios, as well as the effect of core flow mixture ratio variations on temperature and performance at constant barrier flow rates. This allowed the determination of the incremental effect of the two variables—barrier flow rate and core mixture ratio—on performance and heat transfer. Very good correlations were obtained. The effect of design modifications in the vortex barrier injection were also investigated. This paper will present the results of these experimental investigations and the correlation achieved.

Nomenclature

A_i, A_o = internal, external surface area of engine
c^* = over-all characteristic velocity
c_b^* = barrier effective characteristic velocity
c_c^* = core effective characteristic velocity
C_p = specific heat
k = thermal conductivity
h_g = heat-transfer coefficient
P_c = chamber pressure
q = heat flux rate
r = core mixture ratio
t = time
Tg, T_w, T_E = gas, wall, ambient environment temperature
V = volume of wall material
$\dot{W}_b$ = barrier flow rate
$\dot{W}_c$ = core flow rate
$\dot{W}_t$ = total propellant flow rate including barrier
x = axial length
ρ = $\dot{W}_b/\dot{W}_t$, $\rho = W_b$ and W_{FBT}.
σ = Stefan–Boltzmann constant
ϵ = emissivity
μ = density of wall material

Presented as Paper 71-676 at the AIAA/SAE 7th Propulsion Joint Specialist Conference, Salt Lake City, Utah, June 14–18, 1971; submitted June 23, 1971; revision received October 18, 1971. The authors wish to acknowledge the assistance of Palumbo and Blessing in the analysis of the heat-transfer data.

* Chief Engineer, Development and Technical. Fellow AIAA.
† Combustion Devices Engineer.

Introduction and Discussion

THE design of high-performance rocket engines requires that a thermal environment be provided near the engine walls which is compatible with the allowable steady-state temperature levels.[1] In general, this necessitates that the thermal potential of the combustion gas near the heat-transfer surfaces be significantly lower than that of the core products. The provision of a thermal barrier entails a loss in performance relative to what one might achieve if it were not needed. Therefore it is important to establish design parameters which permit meaningful tradeoffs between performance loss and acceptable driving temperatures. Two variables were evaluated in this investigation: 1) the type of barrier, i.e., fuel and oxidizer film; and 2) the utilization efficiency of the barrier as effected by its generation and quantity. A figure of merit must be measured in the capability of providing both uniform

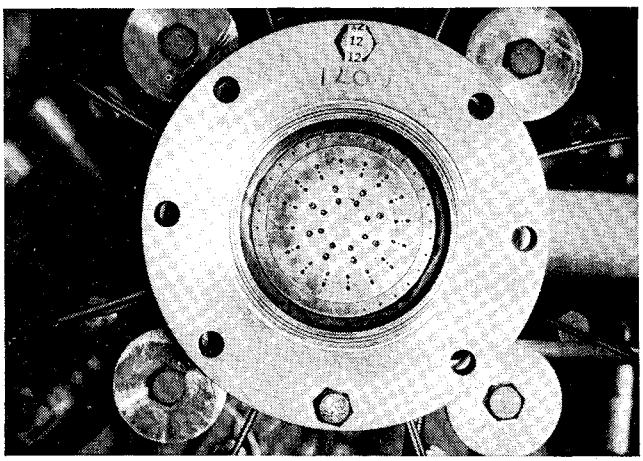

Fig. 1 Injector core and like-on-like doublet face pattern.

thermal protection and minimum performance loss for a desired wall temperature distribution.

This particular investigation was conducted with a nominal 450-lb thrust engine operating at chamber pressures in the range of 100–160 psia. The propellant combination was N_2O_4 and monomethyl hydrazine. The injector was designed to allow the core and barrier flows to be supplied independently of each other. Both fuel and oxidizer were tested as barrier propellants.

Test Hardware and Instrumentation

Injector

An existing injector core of mixed doublet and triplet injection element configuration was selected for this program. Two barrier injector designs—a like-on-like impinging doublet and a vortex sheet—were utilized. The like-on-like doublet barrier injector consisted of a single circumferential row of 32 equally spaced elements. The outer orifice is chamfered and has a diameter of 0.015 in. The inner one has an 0.012-in. diam. A photograph of this assembly is shown in Fig. 1. The vortex barrier injector (Fig. 2) consists of 15 tangential orifices, 0.031 in. in diameter. This figure also shows the relative location of the core and the barrier flows.

Chamber-Nozzle

Chamber sections of 3.4 and 4.5 in. internal diameters and two chamber lengths each were fabricated. In addition, an

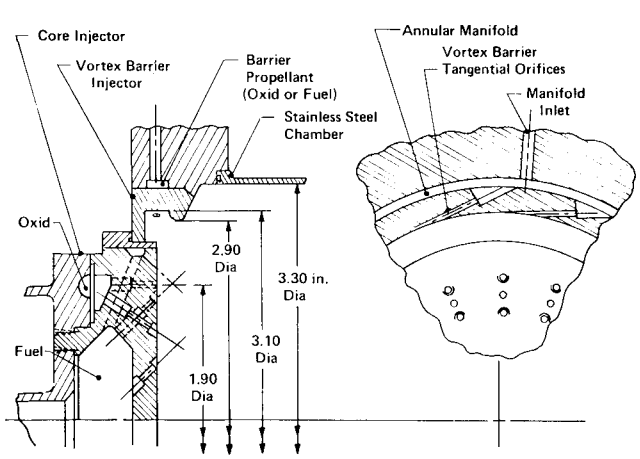

Fig. 2 Vortex barrier injector schematic.

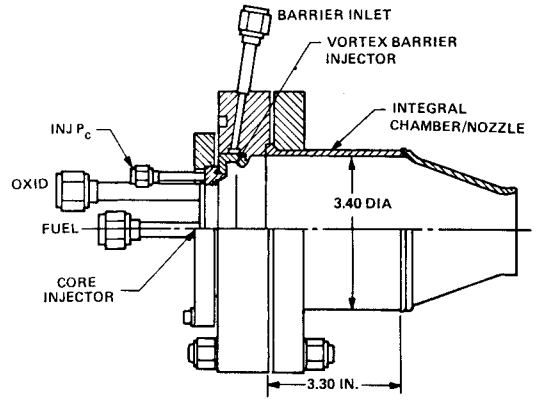

Fig. 3 Vortex barrier and integral s.s. chamber/nozzle.

integral chamber-nozzle configuration (Fig. 3) was built. The two-piece chamber design consisted of a stainless steel combustion chamber section of 0.125 in. wall thickness and a reversible heat sink OFHC copper nozzle which made it adaptable to the two chamber diameters. The integral thrust chamber consisted of a fusion welded stainless steel combustion chamber-nozzle configuration of 3.4 in. chamber diameter and 20 in. L^*. The wall thickness was 0.12 in. and was maintained constant throughout the chamber and nozzle. Although the massive copper heat sink nozzle allowed extended duration tests (i.e. in excess of 30 sec), a compromise in throat thermal data interpretation was incurred. The integral stainless steel chamber-nozzle somewhat rectified this objection although the maximum test duration had to be limited to approximately 10 sec.

Instrumentation

Standard test instrumentation was employed to measure chamber pressure and propellant flow rates. Temperature histories were obtained with chromel-alumel skin thermocouples resistance-welded to the stainless steel chamber walls. The thermocouples were arranged to provide axial as well as tangential profiles of the chamber hardware. The data were recorded on Brush Oscillographs to give real time visual display of temperature rise rates for test termination purposes, and also on a Beckman Model 210 Digital Recording system for permanent record.

Data Analysis

The information one desires is the isolation of the respective effects of core mixture ratio and barrier flow percentage on performance and heat flux. If one assumes a two zone model for the combustor, the following equation can be written:

$$c^* = (c_c^* \dot{W}_c + c_b^* \dot{W}_b)/\dot{W}_t$$
$$= c_c^* + \dot{W}_b/\dot{W}_t\,(c_b^* - c_c^*) = c_c^* + \rho\,(c_b^* - c_c^*) \qquad (1)$$

If the core characteristic velocity is considered to be a function of mixture ratio only, then the slope of the over-all c^* curve can be approximated from Eq. (1) by the expression

$$dc^* = \partial c^*/\partial r dr + \partial c^*/\partial \rho d\rho$$
$$= (1 - \rho)\partial c_c^*/\partial r dr + (c_b^* - c_c^*)d\rho \qquad (2)$$

This expression can be used to evaluate the experimental points, having data at constant core mixture ratio and varying barrier flow ratios or vice versa, to assess the respective performance sensitivity.

Since only transient thermocouple measurements could be obtained with this test hardware, the following assumptions were made to compute the effective gas temperature at the wall and the gas-side heat-transfer coefficient.

A one-dimensional radial heat flow was assumed. Since the heat balance requires that at any instant the heat input to the wall from the combustion gas is equivalent to the sensible heat absorbed by the wall plus the radiant heat lost to the environment, one can write

$$q/A_i = h_g(T_g - T_w) = \mu C_p V/A_i(d T_w/dt) + A_o/A_1\sigma\varepsilon(T_w^4 - T_E^4) \quad (3)$$

where T_w must be considered a mean wall temperature.

From this equality, knowing the wall temperature-time history, the heat rejected to the wall may be obtained as a function of the wall temperature. A straight line representing the solution to the linear equation is fitted through these points and extrapolated to $q/A = 0$. That point represents the local gas driving temperature. The heat-transfer coefficient is the slope of the line

$$h_g = (\Delta q/A)/\Delta T_w \quad (4)$$

Initially, from the various temperatures recorded at the throat station, the extreme data points, i.e., the hottest and coolest at the circumferential locations were used to calculate the convective heating conditions at the throat surface. The following metal wall properties were used: $\mu = 0.29$ lb/in^3, $C_p = 0.13$ Btu/(lb)(°F), $k = 120$ Btu/(hr)(ft^2)(°F)/in.,$\varepsilon = 0.5$.

Since Eq. (3) used to calculate T_g and h_g neglects the thermal gradient through the chamber wall, an adjustment to the analytically determined results is required. This was accomplished by computing one dimensional radial conduction to determine the radial temperature distribution and the outer surface temperature transients for a parametric array of internal boundary conditions. The resulting outer surface temperature transients were in turn used in the heat balance equation to determine the discrepancy between the actual thermal boundary conditions and those predicted by using this equation. For the stainless steel nozzle, it was found that no adjustment in the predicted T_g was required. However, the predicted h_g level had to be increased and this increased correction was incorporated into the calculated values. The correction value is given in Fig. 4.

Subsequently, the heat-transfer coefficients were normalized for the chamber pressure variation between runs. The values for each run were corrected to a chamber pressure of 100 psia, assuming h_g is proportional to $P_c^{0.8}$.

Oxidizer (N_2O_4) Barrier

Oxidizer barrier flow tests were conducted with both the doublet and vortex barrier injectors. These are summarized in Table 1. A wall temperature-time profile of a vortex barrier injector test is shown in Fig. 5. In general, it was observed that the performance and average heat-transfer

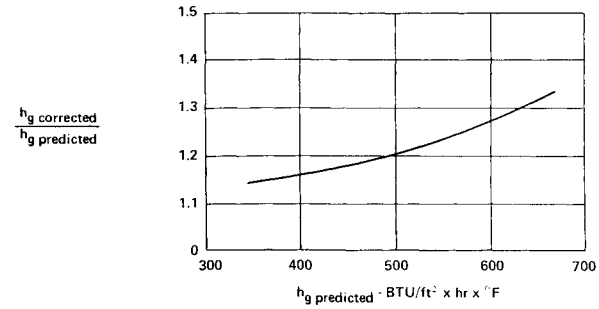

Fig. 4 $H_{g\ \text{pred.}}$ correction for actual thermal boundary conditions.

numbers were very similar for barriers generated by the like-on-like doublets and the vortex; however the uniformity of distribution for the vortex generated barrier was quite superior to that of the doublet. For example, with the doublet, local "hot" spots were encountered near the injector. No such observations were made with the vortex.

In Fig. 6, the over-all characteristic velocity is plotted as a function of barrier flow percentage (ρ) for two different values of core mixture ratios. Although the number of data points obtained is insufficient to make an accurate correlation, the two lines drawn through the data points are: for core mixture ratio of 1.6, $c^* = 5760 - (2350)\rho$; for core mixture ratio of 1.15, $c^* = 5540 - (2200)\rho$. It may be observed that the values appear quite reasonable. For example, oxidizer barrier characteristic velocity c^*_b is calculated to be approximately 3400 fps. It is also noteworthy that the over-all

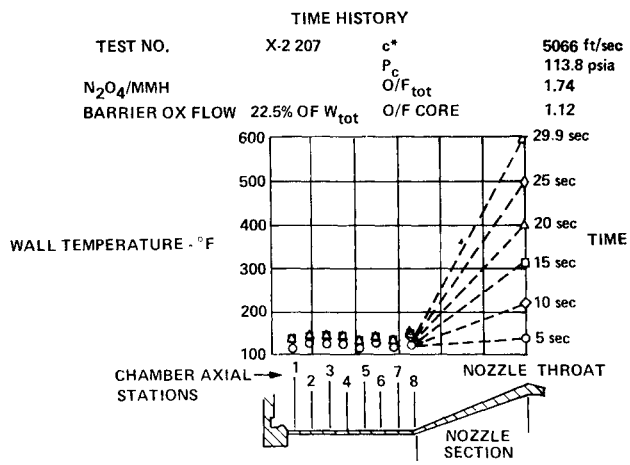

Fig. 5 Local temperature history.

Table 1 Test log—oxidizer barrier

Test duration sec.	Chamber diam, in.	L^*, in.	Barrier type	Total mixture ratio	Core mixture ratio	W_b, lb/sec	W_b/W_t, %	Chamber pressure psia	c^*, fps
3.5	4.5	28	doublet	1.64	1.15	0.302	18.6	105.8	5056
10.8	4.5	28	doublet	1.53	1.08	0.307	17.9	113.9	5145
19.2	4.5	20	doublet	1.59	1.12	0.308	18.3	107.1	4942
9.9	3.4	28	doublet	1.60	1.13	0.309	18.2	112.3	5125
7.2	3.4	28	doublet	2.02	1.57	0.247	14.8	116.7	5422
7.1	3.4	28	doublet	2.17	1.60	0.310	17.9	120.4	5384
8.7	3.4	28	doublet	2.38	1.61	0.420	22.9	124.3	5244
9.8	3.4	28	vortex	2.16	1.60	0.308	17.8	120.5	5406
30.6	3.4	28	vortex	2.31	1.59	0.397	21.8	125.1	5323
30.4	3.4	28	vortex	1.74	1.12	0.402	22.5	116.8	5066
17.9	3.4	28	vortex	1.58	1.11	0.308	18.1	113.2	5141
20.1	3.4	20	vortex	1.57	1.11	0.308	18.1	110.2	5036
18.1	3.4	20	vortex	1.59	1.22	0.255	14.6	116.9	5202

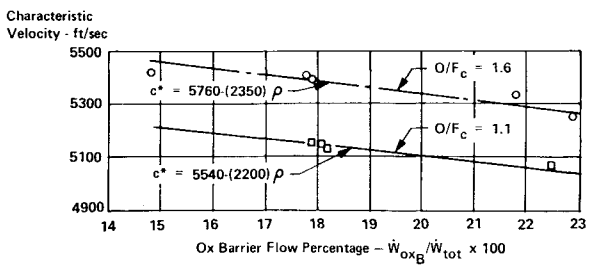

Fig. 6 C^* vs ox barrier flow percentage.

characteristic velocity can indeed be written as a linear relationship of barrier flow ratio, at least within the range evaluated.

The driving temperature and heat-transfer coefficients were computed by means of the techniques described previously. The limited number of data points, however, restricts the accuracy of the values and thus they must be treated with caution. However, gas wall temperatures, Tg, at the throat were calculated as shown in Table 2.

Table 2 Gas wall temperatures at throat (vortex)

Test no.	Temperature, °F
−205	2420
−206	2000
−207	1470
−208	1900
−209	1600
−211	2800

Table 3 Test log—fuel barrier

Total flow mixture ratio	Core mixture ratio	Barrier fuel flow, lb/sec	Chamber pressure, psia	c^*, fps	W_{FB}/W_{tot}, %
1.34	1.82	0.218	122.4	5147	11.4
1.53	2.13	0.195	109.6	5086	11.3
1.53	2.00	0.168	114.3	5174	9.4
1.12	1.99	0.433	108.6	4213	20.8
1.50	1.96	0.165	113.1	5916	9.4
1.61	1.96	0.116	109.8	5268	6.9
1.57	1.95	0.131	111.3	5247	7.7
1.39	1.67	0.120	113.0	5265	7.0
1.80	2.24	0.119	110.0	5160	6.9
1.40	1.96	0.212	114.7	5164	11.9
1.46	1.97	0.187	113.9	5190	10.6
1.52	2.00	0.168	113.1	5200	9.6
1.57	1.98	0.138	112.3	5233	8.0
1.23	1.64	0.211	122.2	5209	11.1
1.28	1.65	0.183	121.0	5230	9.8
1.32	1.65	0.160	120.2	5253	8.7
1.36	1.65	0.136	118.6	5263	7.5
1.62	2.30	0.195	108.2	5071	11.4
1.63	2.28	0.184	107.6	5092	10.8
1.74	2.33	0.155	106.0	5072	9.2
1.80	2.33	0.137	105.2	5088	8.2
1.20	1.64	0.208	159.9	5241	12.1
1.28	1.64	0.239	163.3	5319	9.6
1.34	1.64	0.197	162.1	5344	8.0
1.50	2.12	0.294	162.8	5183	11.6
1.59	2.11	0.237	161.1	5232	9.5
2.03	2.88	0.228	142.0	4877	9.7
2.06	2.85	0.209	140.7	4892	9.0
1.56	1.96	0.194	163.5	5321	7.8
1.61	1.97	0.176	163.2	5328	7.1

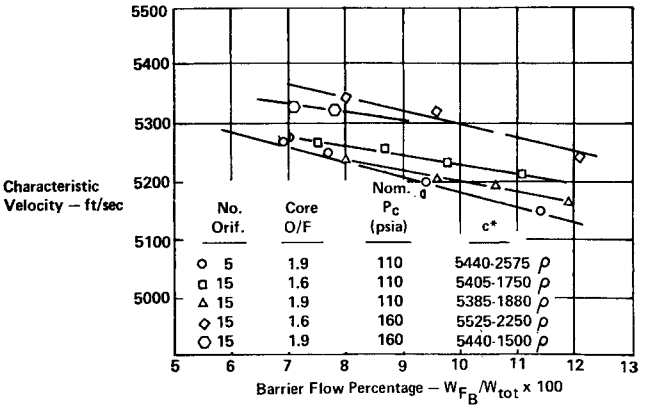

Fig. 7 C^* vs fuel barrier flow percentage (vortex barrier).

Fuel (MMH) Barrier

Fuel barrier tests were conducted only with the vortex injector. The 3.4 in. diam, 20 L^* chamber was used. In order to assess the effect of the vortex momentum, the tangential orifice area was varied in some tests by plugging 10 of the 15 tangential orifices. Nominal chamber pressure levels of 110 psia and 160 psia were evaluated. Table 3 is a compilation of the test series. In Figs. 7 and 8, the over-all characteristic velocity is plotted vs barrier flow rate and barrier flow percentage for various values of core mixture ratio. Figure 9 is a plot of over-all characteristic velocity vs injector core mixture ratio at various barrier flow rates.

Again one can write a linear correlation of over-all c^* vs barrier flow at constant core mixture ratios. These are: 1) for core mixture ratio = 1.9, $P_c = 110$, and 5 tangential vortex orifices, $c^* = 5440 - 2575\rho$; 2) for core mixture ratio = 1.95, $P_c = 110$, and 15 tangential vortex orifices, $c^* = 5385 - 1880\ \rho$; 3) for core mixture ratio = 1.6, $P_c = 110$, and 15 tangential vortex orifices, $c^* = 5405 - 1750\rho$; 4) for

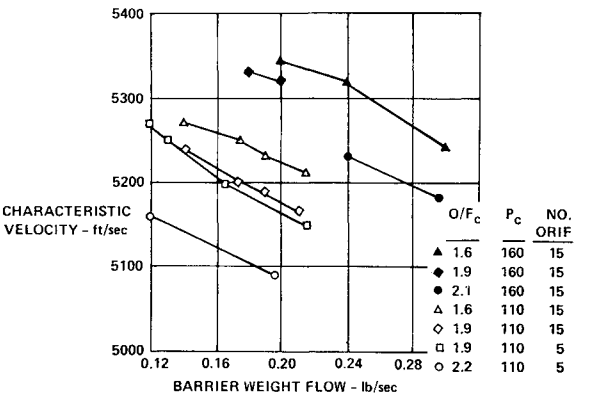

Fig. 8 C^* vs fuel barrier weight flow (vortex).

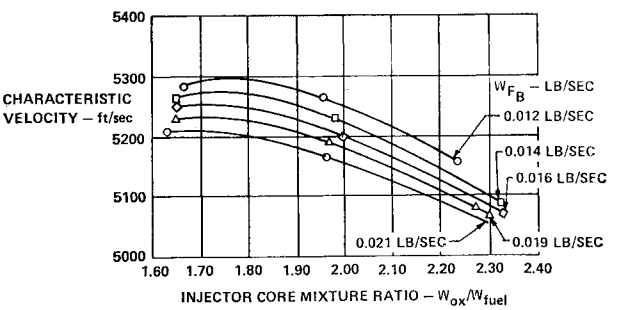

Fig. 9 C^* vs core mixture ratio.

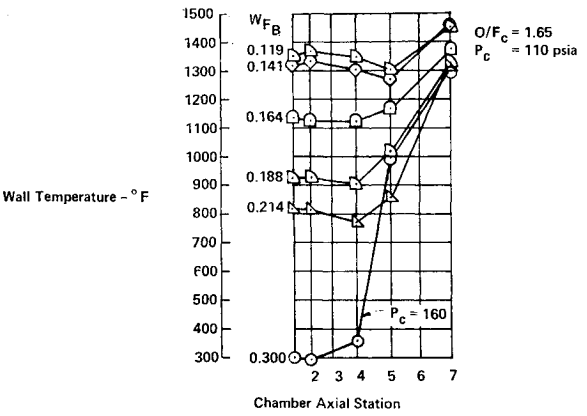

Fig. 10 Wall for various barrier flows at 7 sec.

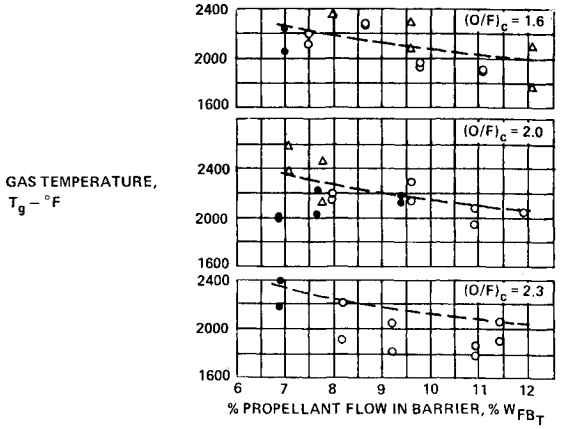

Fig. 12 Throat gas temperature.

core mixture ratio = 1.6, $P_c = 160$, and 15 tangential vortex orifices, $c^* = 5525 - 2250\rho$; 5) for core mixture ratio = 1.9, $P_c = 160$, and 15 tangential vortex orifices, $c^* = 5440 - 1500\rho$. Within the limits of the data range, a linear expression appears fairly adequate. It would appear that the barrier efficiency is reduced for the 5 tangential orifice barrier relative to the corresponding 15 orifice injector.

The wall temperature distribution for fuel barrier cooling is, of course, different than that attained with oxidizer since MMH will undergo monopropellant decomposition. For example, if one assumes that MMH will decompose spontaneously at 600°F to a 2000°F gas, then the following analysis can be made: starting at a nominal temperature of 75°F and a constant pressure of 100 psia, the enthalpy change of N_2O_4 to 2000°F is 1151 Btu/lb whereas for MMH it is 635 Btu/lb. However, for the same temperature increase from 75°F to 600°F, the ΔH of MMH is slightly better, 635 Btu/lb, compared to 563 Btu/lb for N_2O_4. The respective enthalpy change represents only a part of the story in a complete analysis of the relative merits. The effective Nusselt and Prandtl numbers of the generated gas films must also be taken into account. Furthermore, the effect of the respective striated flowfields on nozzle thrust coefficient might become a significant factor for consideration.

Figure 10 shows a typical axial wall temperature profile for various barrier flow rates. Figure 11 depicts the resulting heat-transfer coefficients for three core mixture ratios as functions of the percentage of propellant used in the barrier. The test data, as noted by the symbols in the figure, were segregated into 5 and 15 orifice barrier groups and also 105–125 and 160–165 psia chamber pressure levels. The average value for each mixture ratio is shown by the dashed lines. The over-all average throat h_g is 557 Btu/ft²hr°F. It is interesting to note that there is no correlation between the heat-transfer coefficient and core mixture ratio. Whether this is an indication of the insensitivity of the thermal boundary layer or is a result of the restricted range of test variables cannot be established.

The computed hot gas temperatures are also plotted as a function of percentage of propellant in the coolant barrier. These are shown in Fig. 12. Although the data generally indicate a decreasing gas temperature with increasing percentage of barrier flow, a selection of a best fit curve through the calculated data points is to some degree a matter of judgment. In order to establish a better relationship, the heat flux to the wall was recalculated at an assumed wall temperature T_w of 1000°F. Figure 13 depicts the resulting q/A as a function of percentage of propellant in the barrier. Since this data is not quite as dispersed as the T_g data of Fig. 12, curve fits were conservatively faired through the upper set of data points. These q/A curves used in conjunction with the average heat-transfer coefficient of 557 Btu/ft²hr°F provide the faired-in gas temperature curves in Fig. 12.

In addition to the throat station, an axial location in the chamber section just upstream of the convergent section (station 4) was evaluated. The hottest temperature transients at this station for each of the test runs were similarly used to obtain the data presented in Fig. 14–16. The average heat-transfer coefficient at this station was 331 Btu/ft²hr°F.

Comparing Figs. 12 and 15, it it seen that the predicted gas temperature at station 4 is higher than at the throat station by as much as 400°F for 7% barrier flow and 100°F for 12% barrier. This apparently is caused by local nonuniform heating present in the chamber. It is interesting to note that significant differences were recorded among thermocouple reading at a given axial chamber station, whereas at the throat much better uniformity was observed.

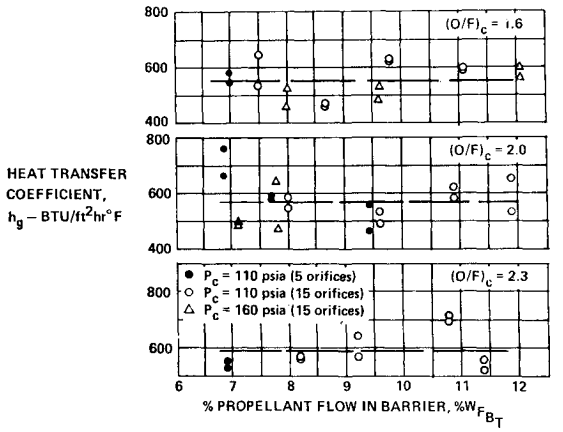

Fig. 11 Throat h_g corrected to $P_c = 100$ psia.

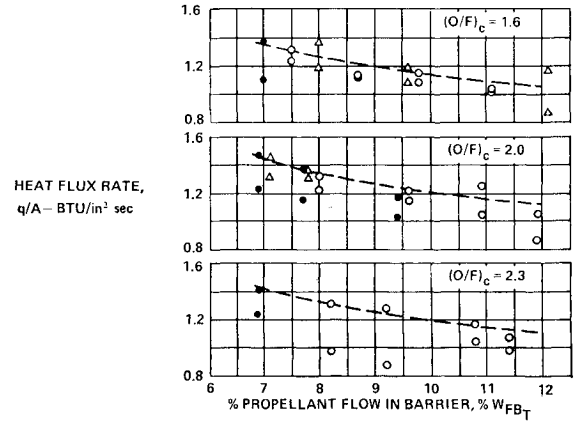

Fig. 13 Throat q/A for 1000°F wall and $P_c = 100$ psia.

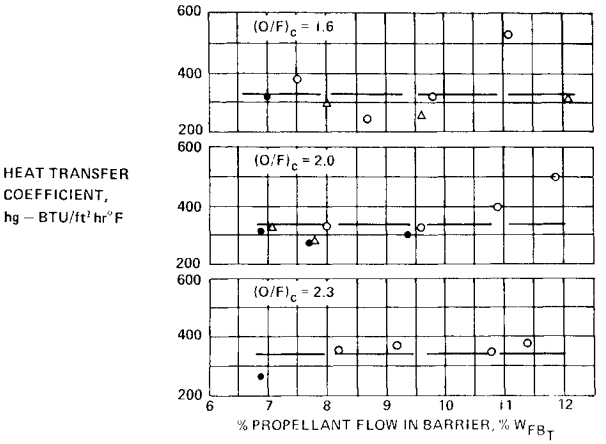

Fig. 14 Station 4 h_g corrected to $P_c = 100$ psia.

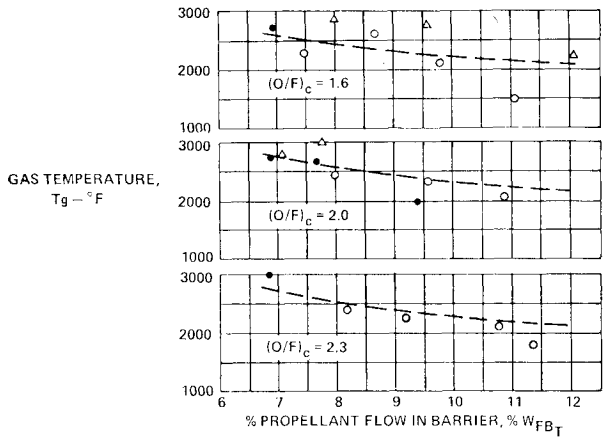

Fig. 15 Station 4 gas temperature.

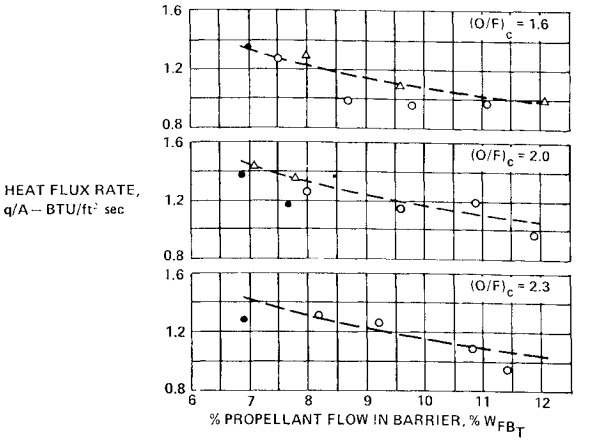

Fig. 16 Station 4 q/A for 500°F wall and $P_c = 100$ psia.

Conclusions

The barrier cooling experiments conducted with N_2O_4 and MMH, respectively, with a nominal 450-lb thrust N_2O_4-MMH engine indicate that low barrier driving temperatures can be achieved and maintained by means of film cooling using either N_2O_4 or MMH. Within the range of barrier flow rates investigated, the c^* performance decreases linearly with the percentage of barrier flow. The barrier is maintained through the nozzle with a calculated gas-side driving temperature nearly equal to the decomposition temperature of MMH. In general, the driving temperatures increase somewhat as the barrier flow rate decreases. Values of gas side heat-transfer coefficients in the chamber and throat were derived. These were relatively independent of core mixture ratio and barrier flow rate. With MMH film cooling, the average throat film cooling coefficient h_g was 557 Btu/ft²hr°F. In the chamber, the value was about 331 Btu/ft²hr°F.

Reference

[1] Stechman, R. C., Oberstone, J., and Howell, J. C., *Journal of Spacecraft and Rockets*, Vol. 6, No. 2, Feb. 1969, pp. 97–102.